Journal of Power Sources 195 (2010) 8215–8221

Contents lists available at ScienceDirect

Journal of Power Sources

journal homepage: www.elsevier.com/locate/jpowsour

# Hydrogen storage properties of $TiMn_{1.5}V_{0.2}$-based alloys for application to fuel cell system

Fang Fang[a], Yongtao Li[a], Qingan Zhang[b], Liangliang Sun[c], Zongping Shao[c], Dalin Sun[a,*]

[a] Department of Materials Science, Fudan University, 220 Handan Road, Shanghai 200433, China
[b] School of Materials Science and Engineering, Anhui University of Technology, Maanshan 243002, China
[c] College of Chemistry and Chemical Engineering, Nanjing University of Technology, Nanjing 210009, China

ARTICLE INFO

*Article history:*
Received 24 April 2010
Received in revised form 16 June 2010
Accepted 17 June 2010
Available online 25 June 2010

*Keywords:*
Ti–Mn-based alloy
Hydrogen absorption/desorption
Hydrogen supply
Hydrogen storage tank

ABSTRACT

To meet the requirements of fuel cell power system for electric bike, the influence of partial substitution of Zr and Cr on hydrogen storage performance of $TiMn_{1.5}V_{0.2}$-based alloys is investigated first, and a hydrogen storage tank is then built using the developed $TiMn_{1.5}V_{0.2}$-based alloy as metal hydride bed and its hydrogen supply ability is further evaluated. It is found that for $TiMn_{1.5}V_{0.2}$-based alloys, the Zr substitution for Ti effectively reduces the plateau pressure but increases the plateau slope, while the partial substitution of Mn by Cr decreases the absorption plateau pressure, leading to a smaller hysteresis factor. After the optimization of components, 6 kg of $Ti_{0.95}Zr_{0.05}Mn_{1.4}Cr_{0.1}V_{0.2}$ alloy powder with 5 wt.% aluminum foam is mixed uniformly to form a metal hydride bed inside the tank. The measurements show that the tank releases up to 82 g of hydrogen to produce a 200 W fuel cell output for 300 min and has a stable cyclic capacity, indicating that hydrogen storage system of $TiMn_{1.5}V_{0.2}$-based alloys for fuel cell power system of electric bike is applicable.



## 1. Introduction

In the last two decades, electric bikes and scooters (for short: E-bikes) have attracted intense attention, due to their low energy consumption and zero tail-pipe emissions [1,2]. More than 90% of E-bikes are driven by valve-regulated lead acid (VRLA) batteries. However, low energy density and environmental issues of VRLA batteries block its development as mobile power systems in the future [2]. This has in turn led to increasing interest in fuel cell powered E-bike, which is expected to offer higher energy density and meet the growing demand for environmentally clean fuels.

At present, on a fuel cell powered E-bike for sale, fuel cell power system mainly consists of high pressure tank and fuel cells. Compared with the high pressure hydrogen, hydrogen stored in metal hydride is regarded as having more potential for mobile applications owing to its advantages in safety and reliability [3–7] and become one of the most powerful technology barriers to the widespread acceptance of hydrogen as an energy vector for automotive applications [8–11]. Recently, metal hydride tanks filled with the conventional $AB_5$-type intermetallics [12–14], alanates [15,16] or $MgH_2$ [17] were prepared and investigated for use as hydrogen sources for proton exchange membrane fuel cells (PEMFC). Several numerical and experimental studies have been reported and focused on improving the structure inside metal hydride tanks to enhance heat and mass transfer properties. By contrast, direct experimental studies on the hydrogen storage performance of metal hydride beds are rarely reported. The metal hydride bed formed by $AB_5$-type intermetallics provides low hydrogen yield (about 1 wt.%) and that formed by alanates or $MgH_2$ release hydrogen at a high temperature of 473–573 K, suggesting that a new materials should be developed to form metal hydride beds to meet the requirements of fuel cell power system at room temperature (RT).

Substoichiometric $TiMn_{1.5}$-based Laves phase alloys are more promising metal hydrides to manufacture the metal hydride bed, due to their high hydrogen storage capacity at RT, easy activation and relatively low cost [18–24]. However, poor plateau characteristics are the stumbling blocks to their development as hydrogen sources for fuel cell systems [25,26]. To overcome these shortfalls, the partial substitution for Ti or Mn was attempted. For example, the hydrogen absorption capacity of $Ti_{1-x}Zr_xMn_\alpha$ ($1.4 \le \alpha \le 1.9$, $0.05 \le x \le 0.4$) increased with enhancing Zr content, but the desorption capacity reached its maximum with $x = 0.1$ [18,27]. In the case of partial substitution for Mn, the plateau pressure of $TiMn_{\alpha-y}M_y$ alloys ($1.3 \le \alpha \le 1.5$, $0.1 \le y \le 0.5$, M = Cu, Co, Fe, Ni, V, Cr) increased when Mn was replaced by Cu, Co or Fe, but decreased when replaced by Ni, Cr or V [18,19]. Moreover, multicomponent alloys such as $TiMn_{1.25-x}Cr_{0.25}V_x$ ($x = 0$, 0.2, 0.3, 0.4, 0.5) [28], $TiV_{0.6}Fe_{0.15}Mn_{1.3}$

* Corresponding author. Tel.: +86 21 65642873; fax: +86 21 65642873.
*E-mail address:* dlsun@fudan.edu.cn (D. Sun).

0378-7753/$ – see front matter. 
doi:10.1016/j.jpowsour.2010.06.059

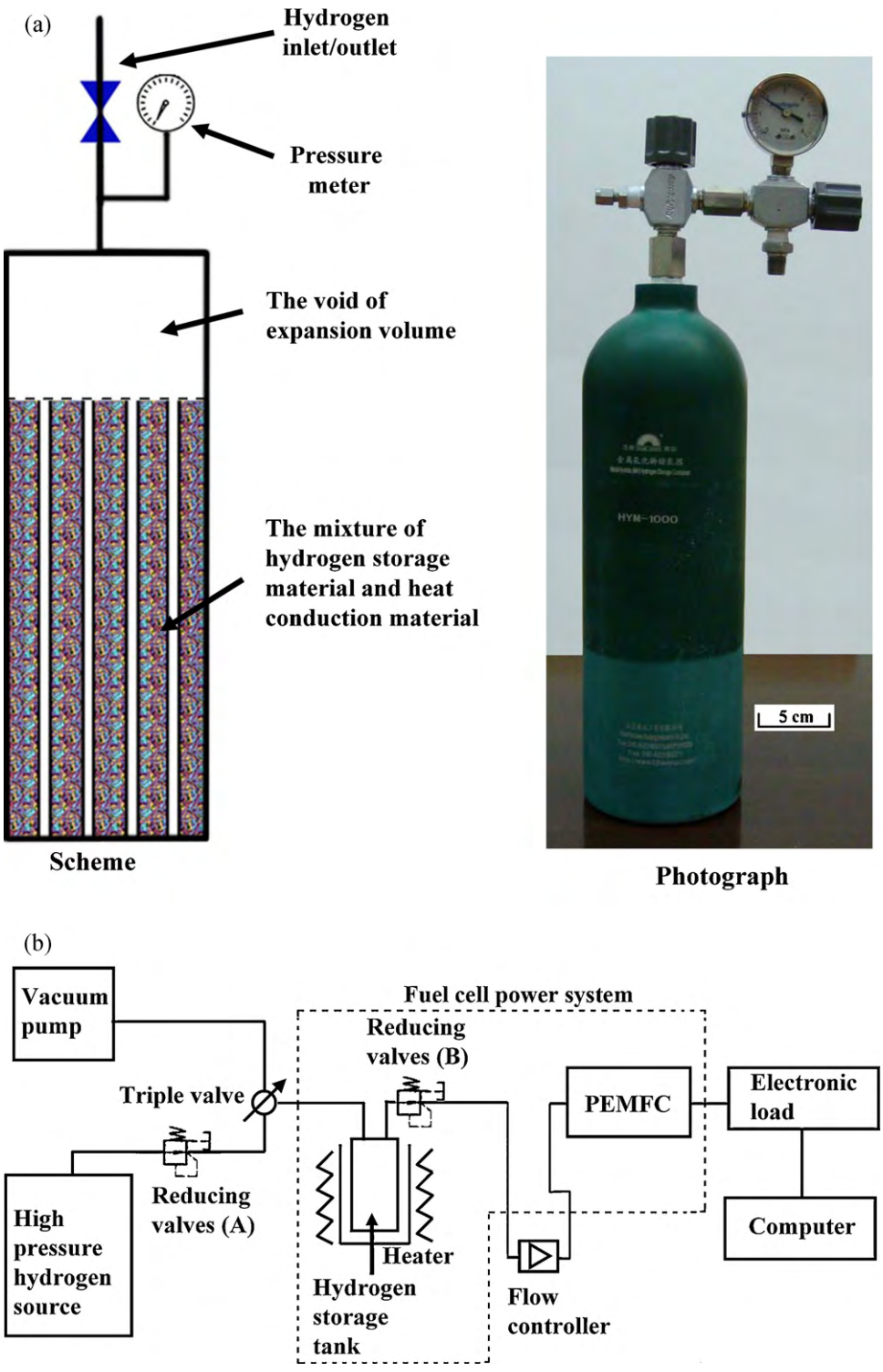


**Fig. 1.** The simplified scheme and photograph of the hydrogen storage tank (a) and the schematic diagram of the test bench associated with the fuel cell system (b).

[29] and $T_{0.95}Zr_{0.05}Mn_{1.45}M_{0.5}$ (M = V, Cr, Mn, Co, Ni, Al) [24] were also prepared to improve the hydrogen storage performance. Nevertheless, it is noticed that previous work on the $TiMn_{1.5}$-based alloys was performed mainly in laboratory, but the reports about practical application, such as their use as hydride beds in hydrogen storage tanks for automotive applications, was rather limited [30]. It is significant to adjust hydrogen storage performance of $TiMn_{1.5}$-based alloys, following the demands of fuel cell power systems.

Previous work on $TiMn_{1.5}V_x$ [31] showed that $TiMn_{1.5}V_{0.2}$ alloys presented a single C14 Laves phase and had a maximum hydrogen storage capacity of 1.54 wt.% at 313 K among $TiMn_{1.5}V_x$ ($x$ = 0–0.5). Considering this fact, in the present work, the influence of partial substitution of Ti by Zr and Mn by Cr in $TiMn_{1.5}V_{0.2}$ alloy was investigated systematically to develop a suitable material for metal hydride beds. Based on the experimental results obtained, a hydrogen storage tank was prepared using the $Ti_{0.95}Zr_{0.05}Mn_{1.4}Cr_{0.1}V_{0.2}$ alloy as a metal hydride bed and its hydrogen supply ability as

**Table 1**
The design parameters for the hydrogen storage tank.

| Subject | Parameters |
|---|---|
| Outside diameter | 108 mm |
| Height | 350 mm |
| Wall thickness | 5.4 mm |
| Volume | 2.0 L |
| Material | Aluminum alloy |
| Weight | 2.2 kg |
| Maximum pressurization | 15.0 MPa |
| Filter | 1000 mesh |
| Gas valve | Twin valve |
| Design hydrogen capacity | 800 NL[a] |

[a] NL: volume expressed in liters under standard conditions.

hydrogen source in a fuel cell power system for E-bike application was then evaluated.

## 2. Experimental

### 2.1. Sample preparation

$Ti_{1-x}Zr_xMn_{1.5}V_{0.2}$ ($x$ = 0–0.2) and $Ti_{0.85}Zr_{0.15}Mn_{1.5-y}Cr_yV_{0.2}$ ($y$ = 0.1–0.4) alloys were prepared by induction melting of appropriate amounts of pure metals under an argon atmosphere. Each sample was re-melted twice for homogeneity, and followed by annealing at 1223 K for 7 days under an argon atmosphere. The alloys obtained were then polished to remove the oxide layer and crushed into powders of less than 48 μm. X-ray diffraction (XRD) was performed at room temperature on a Rigaku D/Max 2500 diffractometer using CuKα radiation with a step size of 0.02°. The diffraction patterns were further analyzed by the Rietveld method implemented in the FULLPROF program [32].

Bulk $Ti_{0.95}Zr_{0.05}Mn_{1.4}Cr_{0.1}V_{0.2}$ alloy was prepared by the electromagnetic levitation melting, followed by annealing, polishing, and crushing as mentioned above. Six kilograms of $Ti_{0.95}Zr_{0.05}Mn_{1.4}Cr_{0.1}V_{0.2}$ alloy powder were mixed uniformly with aluminum foam (5 wt.%) in a nitrogen-filled glove box. The aluminum foam was added to increase heat exchange and to accelerate hydrogen transport during the hydrogenation/dehydrogenation processes.

### 2.2. Sample activation and characterization

Sample powders were loaded into a stainless steel reactor and evacuated at 473 K for 2 h. Hydrogen gas with a pressure of 4 MPa and 0.001 MPa was introduced into the reactor at 313 K for hydriding and dehydriding, respectively. This preliminary hydriding/dehydriding cycling was repeated until a constant value of absorbed hydrogen was obtained. After full activation, the hydrided samples were held under a vacuum at 473 K to remove the hydrogen completely, and then cooled down to RT. Finally, the absorption/desorption kinetics at 273 K, 300 K and 313 K and the pressure–composition isotherm ($P$–$C$ isotherm) at 313 K were measured using a Sieverts-type apparatus.

### 2.3. Preparation and practical test for hydrogen storage tank

The scheme and photograph for the hydrogen storage tank are shown in Fig. 1a and its design parameters are listed in Table 1. The weight, volume and hydrogen capacity of this tank are designed following the requirements of E-bike [1,2]. The hydrogen storage tank was comprised of a cylindrical metal hydride bed and a void of expansion volume atop the metal. The expansion volume was considered as a domain of pure hydrogen gas. Six kilograms of $Ti_{0.95}Zr_{0.05}Mn_{1.4}Cr_{0.1}V_{0.2}$ alloy powder with 5 wt.% aluminum foam was mixed uniformly to form a metal hydride bed inside the tank and the void of expansion volume was estimated to be 1 L, due to the density of about 6.3 g cm$^{-3}$ for the hydride bed. Subsequently, the hydrogen storage tank processed three hydrogenation/dehydrogenation cycles at 313 K (4 MPa for hydrogenation and 0.001 MPa for dehydrogenation) for activation and removal of inert gas.

The simplified scheme of the test bench is shown in Fig. 1b, in which the fuel cell power system is composed of a hydrogen storage tank, a pressure-reducing valve and a PEMFC. Under the conditions of self-humidification and ordinary-press air as the oxidizer, the PEMFC was operated with a purge valve which opened for 0.5 s at 15 s intervals at the ambient temperature. According to the common output power and voltage of VRLA batteries for E-bikes, a PEMFC with 220 W rated power was chosen and operated under constant voltage mode to output 36 V. Since this 220 W PEMFC required a hydrogen source with 0.14–0.2 MPa gas pressure, a pressure-reducing valve (marked as valve B in Fig. 1b) was used to limit the export $H_2$ pressure of tank to 0.15 MPa through the whole hydrogen release process. With the aid of a computer-controlled electronic load and a flow meter, the hydrogen supply ability of the tank in a fuel cell power system for E-bike application was evaluated experimentally by hydrogen pressure inside the tank (recorded per 5 min), hydrogen flow, and the output power of PEMFC.

## 3. Results and discussion

### 3.1. The effect of partial substitution of Ti by Zr

Fig. 2a shows the XRD patterns of $Ti_{1-x}Zr_xMn_{1.5}V_{0.2}$ ($x$ = 0.05–0.20) alloys. It can be seen that only a single C14 Laves phase existed, which suggested that Zr atoms partially replaced Ti and occupied the corresponding positions in the C14 structure. The calculated cell volumes for $Ti_{1-x}Zr_xMn_{1.5}V_{0.2}$ ($x$ = 0.05–0.20) alloys are shown in Fig. 2b. It can be found that the cell volume increased linearly with increasing Zr content, due to larger atomic radius of Zr than Ti atoms.

The absorption/desorption $P$–$C$ isotherms of $Ti_{1-x}Zr_xMn_{1.5}V_{0.2}$ ($x$ = 0–0.20) alloys at 313 K are shown in Fig. 3. With increasing Zr content, the hydrogen capacity increases while the plateau pressure decreases. The increase in hydrogen capacity can be attributed to the fact that the affinity of Zr for H is stronger than that of Ti for H. The decrease in plateau pressure can be explained by the larger cell volume induced by Ti substituted by Zr, which is beneficial to hydrogen absorption/desorption. However, the hydrogen absorption–desorption plateau slope increased with enhancing Zr content. In general, it is realized that plateau slope is significantly affected by the lattice strain in alloys, which can be estimated by the full width at half maximum (FWHM) of the X-ray diffraction peaks when the crystallite size is at the micrometer level [33,34]. The FWHM of peaks (1 0 3) in Fig. 2a are shown in Fig. 4, in which the change in FWHM with increasing Zr content suggested that the increasing plateau slope was caused by larger lattice strain. In addition, similar pressure hysteresis phenomenon is observed in Fig. 3 for all $Ti_{1-x}Zr_xMn_{1.5}V_{0.2}$ samples, suggesting that the hysteresis cannot be lessened effectively by Zr replacement. This undesirable phenomenon can be found in most of the Ti–Mn-based Laves phase alloys and thus caused a loss of thermodynamic efficiency [35–37].

Fig. 5a shows the kinetic curves of hydrogen absorption and desorption for $Ti_{1-x}Zr_xMn_{1.5}V_{0.2}$ ($x$ = 0.05–0.20) alloys at 300 K and the absorption/desorption hydrogen capacities are summarized in Table 2. It can be seen that in the absorption process, $Ti_{1-x}Zr_xMn_{1.5}V_{0.2}$ ($x$ = 0.05–0.20) alloys were fully hydrogenated within 1 min. However, in the desorption process, it took 20–30 min

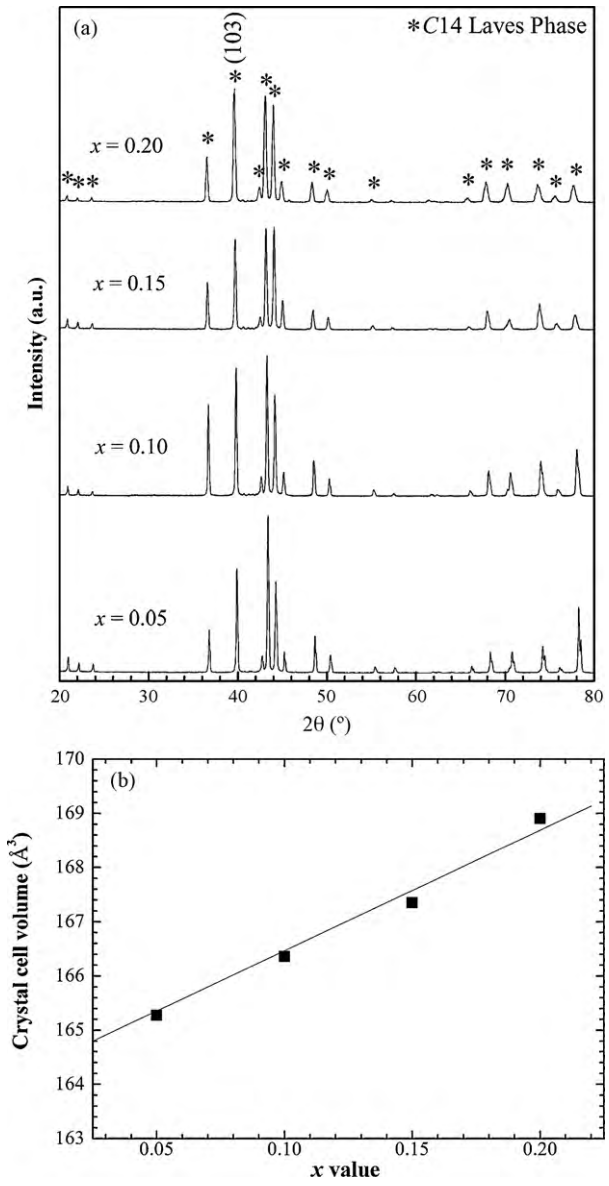


**Fig. 2.** XRD patterns (a) and the calculated cell volume (b) of $Ti_{1-x}Zr_xMn_{1.5}V_{0.2}$ ($x$ = 0.05(0.20) alloys.

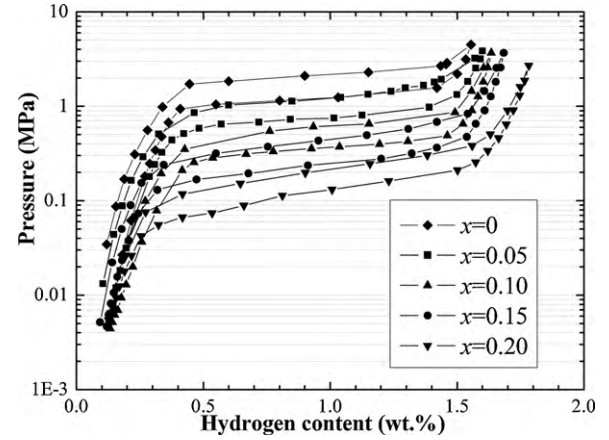


**Fig. 3.** The absorption/desorption $P$–$C$ isotherms for $Ti_{1-x}Zr_xMn_{1.5}V_{0.2}$ ($x$ = 0(0.20) alloys at 313 K.

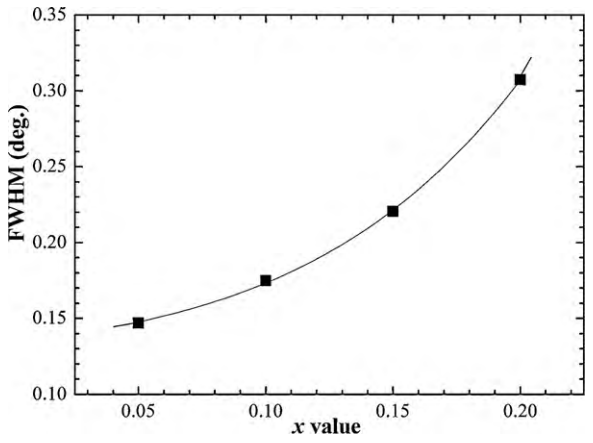


**Fig. 4.** The changes of FWHM as a function of $x$ value for $Ti_{1-x}Zr_xMn_{1.5}V_{0.2}$ ($x$ = 0(0.20) alloys.

to complete the hydrogen release process. Moreover, as Table 2 shows, although the absorption and desorption hydrogen capacity increased from 1.60 wt.% to 1.79 wt.% and 1.49 wt.% to 1.60 wt.% with increasing Zr content, respectively, the capacity ratio of desorption to absorption decreased from 93.1% to 89.4%, probably due to the formation of stabilized Zr-hydride. To check the impact of temperature on kinetics, the absorption/desorption kinetics of $Ti_{1-x}Zr_xMn_{1.5}V_{0.2}$ ($x$ = 0.05–0.20) alloys were further investigated at 273 K, 300 K and 313 K. As a typical example, the kinetics curves for $Ti_{0.95}Zr_{0.05}Mn_{1.5}V_{0.2}$ alloy are shown in Fig. 5b. It can be seen that $Ti_{0.95}Zr_{0.05}Mn_{1.5}V_{0.2}$ alloy had excellent absorption kinetics at 273–313 K, but desorption kinetics was degraded to some extent

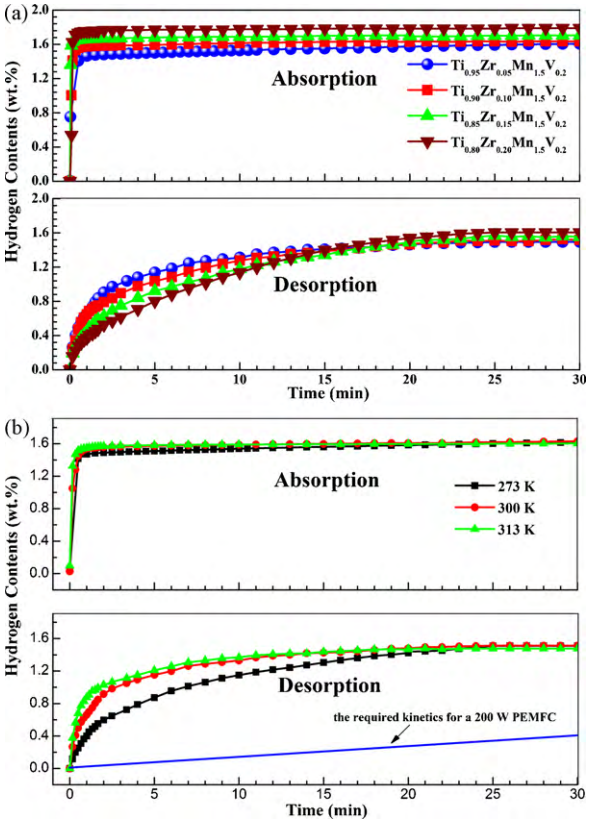


**Fig. 5.** The hydrogen absorption/desorption kinetics for $Ti_{1-x}Zr_xMn_{1.5}V_{0.2}$ ($x$ = 0.05(0.20) alloys at 300 K (a) and $Ti_{0.95}Zr_{0.05}Mn_{1.5}V_{0.2}$ alloy at 273 K, 300 K and 313 K (b).

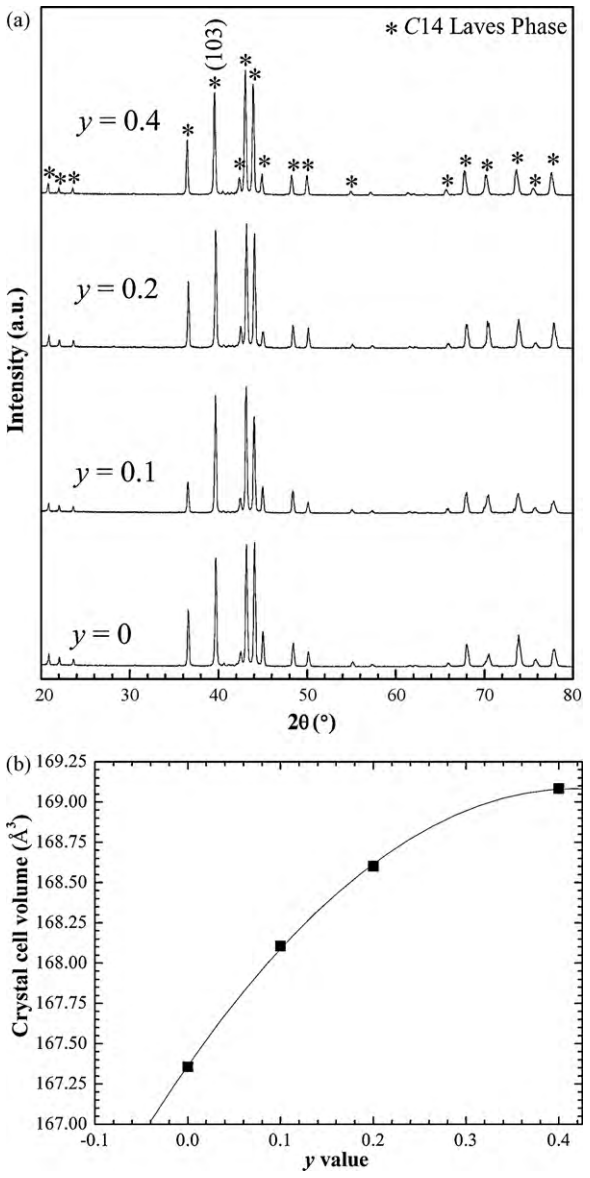


**Fig. 6.** The XRD patterns (a) and calculated cell volume (b) of $Ti_{0.85}Zr_{0.15}Mn_{1.5-y}Cr_yV_{0.2}$ ($y$ = 0(0.4) alloys.

when the temperature decreased to 273 K, owing to the endothermic dehydrogenation. From this result, a question raised is whether such desorption kinetics meet the demand of a 200 W PEMFC system. In theory, a hydrogen source for a 200 W PEMFC system requires a 3 NL min$^{-1}$ hydrogen flow [38]. Considering the 1.2 wt.% design capacity (800 NL) of the hydrogen storage tank in this study, the required desorption kinetics of metal hydride bed is 0.0045 wt.% min$^{-1}$ and is shown in Fig. 5b. It can be seen that the desorption kinetics of $Ti_{1-x}Zr_xMn_{1.5}V_{0.2}$ ($x$ = 0.05–0.20) alloys evidently meet the requirement for a 200 W PEMFC system in the temperature range 273–313 K.

### 3.2. The effect of partial substitution of Mn by Cr

To lessen the hysteresis observed in Fig. 3, the influence of partial substitution of Cr for Mn on the hydrogen storage properties of $Ti_{0.85}Zr_{0.15}Mn_{1.5}V_{0.2}$ alloy was further investigated. The XRD patterns and the calculated cell volume of $Ti_{0.85}Zr_{0.15}Mn_{1.5-y}Cr_yV_{0.2}$ ($y$ = 0–0.4) alloys are shown in Fig. 6a and b, respectively. Similar to that observed in $Ti_{1-x}Zr_xMn_{1.5}V_{0.2}$ ($x$ = 0.05–0.20) alloys, single C14

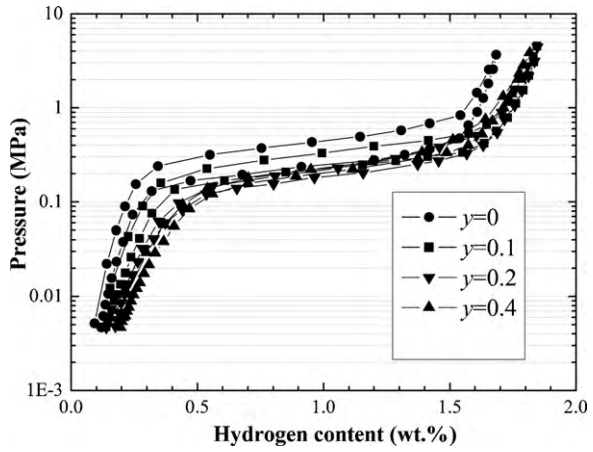


**Fig. 7.** The absorption/desorption $P$–$C$ isotherms for $Ti_{0.85}Zr_{0.15}Mn_{1.5-y}Cr_yV_{0.2}$ ($y$ = 0(0.4) alloys at 313 K.

Laves phase and the increasing cell volume were observed in the Cr-substituted alloys. Though Cr has a smaller atomic radius than Mn ($r_{Cr}$ = 1.27 Å, $r_{Mn}$ = 1.32 Å), the cell volume still increased with increasing Cr content, which may be attributed to their electronic structure [18,39].

The absorption/desorption $P$–$C$ isotherms for $Ti_{0.85}Zr_{0.15}Mn_{1.5-y}Cr_yV_{0.2}$ ($y$ = 0–0.4) alloys at 313 K are shown in Fig. 7, from which two features can be seen: (i) with increasing Cr content, the absorption plateau pressure decreased while the desorption plateau pressure was invariable, leading to a smaller hysteresis factor. This may be explained by the smaller hysteresis factor reported for $TiCr_2$ compared with that for $TiMn_2$ [5,24]; (ii) the maximum hydrogen capacity increased from 1.64 wt.% ($y$ = 0) to 1.83 wt.% ($y$ = 0.1–0.4). The excessive Cr content ($y$ is more than 0.1) could not further increase the capacity, but reduced the hydrogen absorption–desorption plateau region, which greatly decreased the reversible hydrogen storage capacity.

In addition, the kinetic curves of hydrogen absorption and desorption for $Ti_{0.85}Zr_{0.15}Mn_{1.5-y}Cr_yV_{0.2}$ ($y$ = 0–0.4) alloys at 313 K are shown in Fig. 8a and those for $Ti_{0.85}Zr_{0.15}Mn_{1.4}Cr_{0.1}V_{0.2}$ alloy at 273 K, 300 K and 313 K are presented in Fig. 8b. It can be seen that $Ti_{0.85}Zr_{0.15}Mn_{1.5-y}Cr_yV_{0.2}$ ($y$ = 0–0.4) alloys had fast absorption kinetics at 273–313 K and exhibited a slight degradation of desorption kinetics at 273 K, similar to those of $Ti_{1-x}Zr_xMn_{1.5}V_{0.2}$ ($x$ = 0.05–0.20) alloys. The absorption/desorption hydrogen capacities for Fig. 8a are also summarized in Table 2. The capacity ratio of desorption to absorption decreased from about 92.0% ($y$ = 0 and 0.1) to 88.5% ($y$ = 0.2 and 0.4), due to the narrow plateau of $Ti_{0.85}Zr_{0.15}Mn_{1.5-y}Cr_yV_{0.2}$ ($y$ = 0.2 and 0.4).

### 3.3. Hydrogen supply property in a fuel cell power system

Based on the results above, $Ti_{0.95}Zr_{0.05}Mn_{1.4}Cr_{0.1}V_{0.2}$ alloy was selected for the manufacture of a metal hydride bed in a hydrogen storage tank for the following three reasons: (i) the alloy can provide about 3 NL min$^{-1}$ hydrogen flow for a 200 W PEMFC (see Figs. 5 and 8); (ii) reasonable Cr content lessens the hysteresis of plateau pressure and increases the reversible hydrogen storage capacity; and (iii) PEMFC requires a hydrogen source with 0.14–0.2 MPa gas pressure. Considering the reduction of plateau pressure by introducing Cr into $Ti_{1-x}Zr_xMn_{1.5}V_{0.2}$ alloys, the value 0.05 was chosen for $x$ to ensure that the pressure remained above 0.15 MPa at 300 K when the hydrogen content decreased to 0.3 wt.%. Referring to Figs. 3, 7 and 8, the metal hydride bed was expected to possess a 0.2–0.9 MPa plateau pressure, 10 min hydrogen loading time and 1.5 wt.% available hydrogen capacity (without consid-

**Table 2**
The hydrogen absorption/desorption capacity of $Ti_{1-x}Zr_xMn_{1.5}V_{0.2}$ ($x$ = 0.05–0.2) and $Ti_{0.85}Zr_{0.15}Mn_{1.5-y}Cr_yV_{0.2}$ ($y$ = 0–0.4) in kinetics measurements at 300 K.

| | $Ti_{1-x}Zr_xMn_{1.5}V_{0.2}$ | | | | $Ti_{0.85}Zr_{0.15}Mn_{1.5-y}Cr_yV_{0.2}$ | | | |
|---|---|---|---|---|---|---|---|---|
| Component ($x$ or $y$ value) | 0.05 | 0.1 | 0.15 | 0.2 | 0 | 0.1 | 0.2 | 0.4 |
| Absorption capacity (wt.%) | 1.60 | 1.63 | 1.70 | 1.79 | 1.70 | 1.83 | 1.84 | 1.82 |
| Desorption capacity (wt.%) | 1.49 | 1.52 | 1.56 | 1.60 | 1.56 | 1.70 | 1.62 | 1.61 |
| The capacity ratio of desorption to absorption (%) | 93.1 | 93.3 | 91.8 | 89.4 | 91.8 | 92.9 | 88.0 | 88.5 |

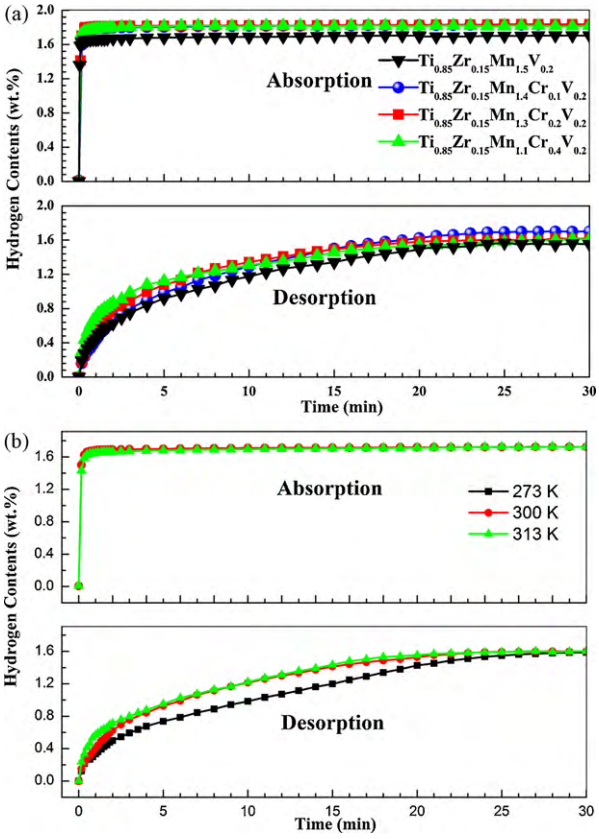


**Fig. 8.** The kinetics of hydrogen absorption and desorption for $Ti_{0.85}Zr_{0.15}Mn_{1.5-y}Cr_yV_{0.2}$ ($y$ = 0(0.4) alloys at 300 K (a) and for $Ti_{0.85}Zr_{0.15}Mn_{1.4}Cr_{0.1}V_{0.2}$ alloy at 273 K, 300 K, and 313 K (b).

eration of hydrogen capacity when plateau pressure is below 0.15 MPa).

Fig. 9 shows the PEMFC output power and the hydrogen pressure inside the hydrogen storage tank as a function of release time.

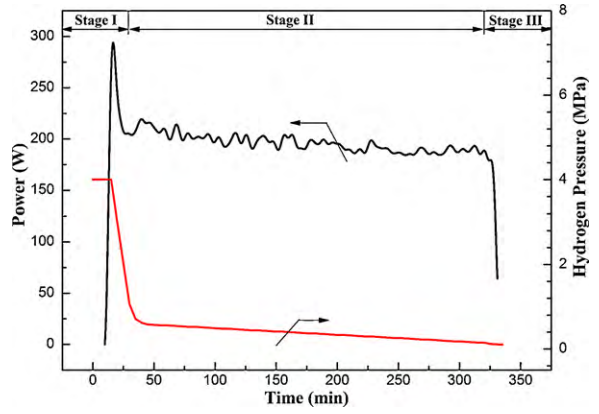


**Fig. 9.** The output power of PEMFC and the hydrogen pressure inside the hydrogen storage tank as a function of time during release process at 300 K.

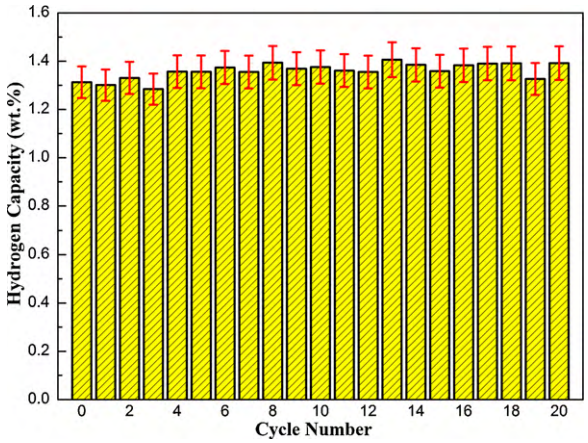


**Fig. 10.** The cycling capacity for hydrogen storage tank at 300 K.

The output process of this PEMFC system can be divided into three stages as marked in Fig. 9: (i) in stage I, the PEMFC output power reduced from 300 W to 205 W within 10 min due to self-humidified technology used in PEMFC, meanwhile the hydrogen pressure in tank declined linearly from 4 MPa to 1 MPa; (ii) in stage II, the output power maintained at about 200 W (185–215 W) for 295 min and the hydrogen pressure declined first to 0.6 MPa and then slowly to 0.15 MPa. The change of hydrogen pressure inside the tank suggested that the metal hydride bed desorbed hydrogen when the hydrogen pressure was below 1 MPa and the equilibrium pressure for hydrogen desorption was in the range of 0.15–0.6 MPa; and (iii) in stage III, the hydrogen pressure was below 0.15 MPa, leading to a rapid decrease of PEMFC output power. After completion of the release process, 920 NL (corresponding to 82.1 g) of hydrogen with an average flow rate of 3 NL $min^{-1}$ was recorded by flow meter. After deducting 2.7–3.6 g (30–40 NL) of hydrogen gas that was stored in the void of expansion volume of the tank, the metal hydride bed could release about 78.6 g (880 NL) hydrogen gas, corresponding to 1.31 wt.% of available hydrogen capacity. This available hydrogen capacity was slightly lower than the expectation of 1.5 wt.% since the equilibrium pressure was lower than that expected and the metal hydride bed inside the tank was difficult to be fully hydrogenated. As a power source for E-bike, with consideration of the total weight of 10.5 kg for the metal hydride tank and PEMFC, the specific energy of this fuel cell power system is calculated to be 95 W h $kg^{-1}$, which was 6–30% higher than that of VRLA batteries (36 V/20 A h, 8–10 kg) [1].

A cycling test was carried out and is shown in Fig. 10. The cycling conditions were maintained at 300 K and 4 MPa for loading and 300 K and 0.15 MPa for releasing. It can be seen that the tank had a stable hydrogen capacity of about 1.33 wt.% throughout 20 cycles. However, it should be noticed that during the cycling test, it took about 2 h, longer than the expectation of 10 min, to complete each loading process, which can be attributed to the slow hydrogen transport inside the tank. Referring to the kinetics measurement in Fig. 8, it can be expected that the reloading time would be greatly shortened by piping hydrogen.

## 4. Conclusions

In summary, to develop a metal hydride bed inside a hydrogen storage tank for fuel cell power system for E-bike application, the effect of Zr and Cr addition on hydrogen storage performance of $TiMn_{1.5}V_{0.2}$-based alloy was studied. The results obtained are as follows: (i) with increasing Zr content in $Ti_{1-x}Zr_xMn_{1.5}V_{0.2}$ ($x$ = 0–0.2), the plateau pressure decreased and the hydrogen storage capacity increased, while the plateau slope increased and the capacity ratio of desorption to absorption decreased. Moreover, a undesirable hysteresis occurred in $Ti_{1-x}Zr_xMn_{1.5}V_{0.2}$ ($x$ = 0–0.2) and thus caused a loss of thermodynamic efficiency; (ii) the partial substitution of Cr for Mn in $Ti_{0.85}Zr_{0.15}Mn_{1.5-y}Cr_yV_{0.2}$ was beneficial to enhancing the hydrogen storage capacity, lessening the hysteresis and improving the desorption kinetics. However, the plateau region narrowed with increasing Cr content, leading to a smaller available hydrogen storage capacity; (iii) with the consideration of design capacity of the hydrogen storage tank, the absorption/desorption kinetics of all samples at 273–313 K met the requirement of a metal hydride bed for 200 W PEMFC. Based on the experimental results, a hydrogen storage tank was built using the mixture of 6 kg $Ti_{0.95}Zr_{0.05}Mn_{1.4}Cr_{0.1}V_{0.2}$ alloy powder with 5 wt.% aluminum foam as the metal hydride bed, and its hydrogen supply ability in a fuel cell power system was evaluated experimentally. The tank could release up to 920 NL of hydrogen (1.31 wt.%) with a 3 NL $min^{-1}$ hydrogen flow and had a stable cycle capacity. The fuel cell power system outputted 200 W for 300 min suggesting that the $TiMn_{1.5}V_{0.2}$-based alloy was a promising material for metal hydride bed in a fuel cell power system for E-bike application.

## Acknowledgements

This work was financially supported by the Ministry of Science and Technology of China (Nos. 2007CB209706 and 2010CB631302) and the National Natural Science Foundation of China (Nos. 20833009 and 50925102).

## References

[1] J.X. Weinert, A.F. Burke, W.Z. Wei, J. Power Sources 172 (2007) 938–945.
[2] Y.L. Guo, S.Q. Tang, G. Meng, S.J. Yang, J. Power Sources 191 (2009) 127–133.
[3] O. Boser, J. Less-Common Met. 46 (1976) 91–99.
[4] S. Fang, Z. Zhou, J. Zhang, M. Yao, F. Feng, D.O. Northwood, Int. J. Hydrogen Energy 25 (2000) 143–149.
[5] B.H. Liu, D.M. Kim, K.Y. Lee, J.Y. Lee, J. Alloys Compd. 240 (1996) 214–218.
[6] S.V. Mitrokhin, T.N. Smirnova, V.A. Somenkov, V.P. Glazkov, V.N. Verbetsky, J. Alloys Compd. 356–357 (2003) 80–83.
[7] L. Schlapbach, A. Züttel, Nature 414 (2001) 353–358.
[8] M. Granovskii, I. Dincer, M.A. Rosen, Int. J. Hydrogen Energy 31 (2006) 337–352.
[9] R. Helmolt, U. Eberle, J. Power Sources 165 (2007) 833–843.
[10] P. Corbo, F.E. Corcione, F. Migliardini, O. Veneri, J. Power Sources 145 (2005) 610–619.
[11] C.A. Chung, C.J. Ho, J. Power Sources 34 (2009) 4351–4364.
[12] M. Botzung, S. Chaudourne, O. Gillia, C. Perret, M. Latroche, A. Percheron-Guegan, P. Marty, Int. J. Hydrogen Energy 32 (2008) 98–101.
[13] K. Akiyama, S. Matsumoto, A. Miyasaka, T. Shodai, J. Power Sources 186 (2009) 37–44.
[14] F. Askri, M. Ben Salah, A. Jemni, S. Ben Nasrallah, Int. J. Hydrogen Energy 34 (2009) 6705–6711.
[15] C. Na Ranong, M. Hoehne, J. Franzen, J. Hapke, G. Fieg, M. Dornheim, N. Eigen, J.M. Bellosta von Colbe, O. Metz, Chem. Eng. Technol. 32 (2009) 1154–1163.
[16] P. Corbo, F. Migliardini, O. Veneri, J. Power Sources 193 (2009) 285–291.
[17] A. Chaise, P. De Rango, Ph. Marty, D. Fruchart, J. Power Sources 35 (2010) 6311–6322.
[18] T. Gamo, Y. Moriwaki, N. Yanagihara, T. Iwaki, Int. J. Hydrogen Energy 10 (1985) 39–47.
[19] X.B. Yu, B.J. Xia, Z. Wu, N.X. Xu, Mater. Sci. Eng. A 373 (2004) 303–308.
[20] S. Semboshi, N. Masahashi, S. Hanada, Acta Mater. 49 (2001) 927–935.
[21] S. Semboshi, M. Sakurai, N. Masahashi, T.J. Konno, S. Hanada, J. Alloys Compd. 376 (2004) 232–240.
[22] B.K. Singh, A.K. Singh, A.M. Imam, O.N. Srivastava, Int. J. Hydrogen Energy 26 (2001) 817–821.
[23] D. Fruchart, J.L. Soubeyroux, R. Hempelmann, J. Less-Common Met. 99 (1984) 307–319.
[24] J.L. Bobet, B. Chevalier, B. Darriet, Intermetallics 8 (2000) 359–363.
[25] H. Nakano, S. Wakao, T. Shimizu, J. Alloys Compd. 253–254 (1997) 609–612.
[26] S.V. Mitrokhin, T.N. Bezuglaya, V.N. Verbetsky, J. Alloys Compd. 330–332 (2002) 146–151.
[27] J.G. Park, H.Y. Jiang, S.C. Han, P.S. Lee, J.Y. Lee, J. Alloys Compd. 325 (2001) 293–298.
[28] X.B. Yu, Z. Wu, Q.R. Chen, T. Dou, J.Z. Chen, B.J. Xia, N.X. Xu, J. Mater. Process. Technol. 182 (2007) 549–554.
[29] J. Toepler, O. Bernauer, H. Buchner, H. Saeufferer, J. Less-Common Met. 89 (1983) 519–526.
[30] Y. Kojima, Y. Kawai, S. Towata, T. Matsunaga, T. Shinozawa, M. Kimbara, J. Alloys Compd. 419 (2006) 256–261.
[31] Y.T. Li, G.Y. Zhou, F. Fang, H.P. Han, Q.A. Zhang, D.L. Sun, J. Mater. Res. 24 (2009) 2886–2891.
[32] H.M. Rietveld, Acta Crystallogr. 22 (1967) 151–152.
[33] J.M. Park, J.Y. Lee, J. Less-Common Met. 167 (1991) 245–249.
[34] D.H. Bradhurst, Met. Forum 6 (1983) 139–148.
[35] Y. Komazaki, M. Uchida, S. Suda, A. Suzuki, S. Ono, N. Nishimiya, J. Less-Common Met. 89 (1983) 269–274.
[36] Y. Moriwaki, T. Gamo, T. Iwaki, J. Less-Common Met. 172–174 (1991) 1028–1035.
[37] S.N. Klyamkin, V.N. Verbetsky, V.A. Demidov, J. Alloys Compd. 205 (1994) L1–L2.
[38] S.G. Chalk, J.F. Miller, F.W. Wagner, J. Power Sources 86 (2000) 40–51.
[39] X.Q. Chen, V.T. Witusiewicz, R. Podloucky, P. Rogl, F. Sommer, Acta Mater. 51 (2003) 1239–1247.